

CCMamba: Selective State-Space Models for Higher-Order Graph Learning on Combinatorial Complexes

Jiawen Chen¹, Qi Shao¹, Mingtong Zhou¹, Duxin Chen^{1, 2*}, Wenwu Yu^{1, 2*}

¹School of Mathematics, Southeast University, Nanjing, Jiangsu, China

²Jiangsu Province Center for Applied Mathematical Sciences, Jiangsu, China

{chenjiawen,shaoqi,213221863,chendx,wwyu}@seu.edu.com

Abstract

Topological deep learning has emerged for modeling higher-order relational structures beyond pairwise interactions that standard graph neural networks fail to capture. Although combinatorial complexes offer a unified topological framework, most existing topological deep learning methods rely on local message passing via attention mechanisms, which incur quadratic complexity and remain low-dimensional, limiting scalability and rank-aware information aggregation in higher-order complexes. We propose Combinatorial Complex Mamba (CCMamba), the first unified mamba-based neural framework for learning on combinatorial complexes. CCMamba reformulates message passing as a selective state-space modeling problem by organizing multi-rank incidence relations into structured sequences processed by rank-aware state-space models. This enables adaptive, directional, and long-range information propagation in linear time without self-attention. We further establish the theoretical analysis that the expressive power upper-bound of CCMamba message passing is the 1-Weisfeiler–Lehman test. Experiments on graph, hypergraph, and simplicial benchmarks demonstrate that CCMamba consistently outperforms existing methods while exhibiting improved scalability and robustness to depth.

1 Introduction

Many real-world systems, ranging from biomolecular interaction networks [Truong and Chin, 2024] to traffic dynamics [Pham *et al.*, 2025], image manifolds [Love *et al.*, 2023], and multi-scale geometric structures, exhibit relational patterns that extend far beyond pairwise interactions. While graphs offer a flexible representation for modeling 1-dimensional relations, they are intrinsically limited in expressing multi-way, hierarchical, and boundary-aware dependencies that arise in higher-order domains such as hypergraphs, simplicial complexes, and cellular complexes. This limitation motivates the proposal of combinatorial complexes (CCs)

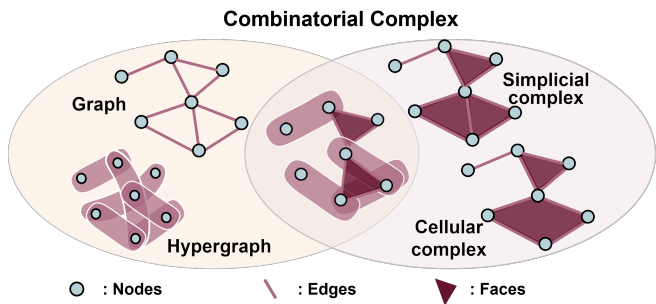


Figure 1: Illustration of combinatorial complex

in Figure 1, which provide a principled topological framework to capture higher-order interactions. CCs organize entities into ranked cells (nodes, edges, faces, etc.) connected via boundary and co-boundary operators [Hajij *et al.*, 2022; Hajij *et al.*, 2023], thereby offering a unified structure that can generalize graphs, hypergraphs, and higher-order complexes. This framework has become frontier to topological deep learning (TDL), enabling modeling of higher-order graphs.

To exploit these structures, a rich family of neural architectures have been proposed. Hypergraph neural networks employ node–hyperedge message passing and have achieved strong performance on node classification tasks [Cai *et al.*, 2022], typically through two-stage aggregation schemes [Feng *et al.*, 2019; Ding *et al.*, 2020; Ding *et al.*, 2023]. However, HGNs primarily model node–edge interactions and consider only low-dimensional, local message passing, leaving higher-order dependencies (e.g. edge–face, multi-rank interactions) unmodeled. Unified approaches like UniGNN [Huang and Yang, 2021], CCNNs [Hajij *et al.*, 2022; Hajij *et al.*, 2023], and the topological message passing framework of TopoTune [Papillon *et al.*, 2023] attempt to generalize beyond hypergraphs. These methods introduce higher-order message passing, but most remain iterative and inherently local [Naitzat *et al.*, 2020; Wen *et al.*, 2024], limiting their ability to capture long-range, directional and fully structured dependencies. These advances demonstrate the value of explicitly modeling structural geometry, yet most of them rely on low-order or graph-based formulations. This limitation highlights the need to move beyond such representations to exploit the geometry learning of higher-order structures in topological deep learning.

*Corresponding author: Duxin Chen, Wenwu Yu.

Parallel to these developments, a series of recent works has explored new perspectives on topological deep learning and the integration of topological priors into neural architectures. Prior works like MPSNs [Bodnar, 2023], which extend cellular complexes via algebraic topology, formalize message passing in terms of node-edge-face interactions. Similarly, simplicial neural networks (SNNs) [Roddenberry *et al.*, 2021; Lecha *et al.*, 2025], SCNNs [Wu *et al.*, 2023], cellular neural networks [Bodnar *et al.*, 2021], and TopoTune [Battiloro *et al.*, 2024] extend message passing to simplicial and cellular complexes, leveraging algebraic-topological operators to capture higher-order interactions. Although effective, these approaches are tied to specific complex types and typically overlook asymmetric or directional flows across ranks [Hajij *et al.*, 2022; Hajij *et al.*, 2023]. Recent attempts extend attention and transformer-style architectures [Papamarkou *et al.*, 2024; Papillon *et al.*, 2025; Bick *et al.*, 2024] on hypergraph, simplicial complex. However, these transformer-based methods remain inherently low-dimensional in their message passing, and the quadratic complexity of self-attention makes them difficult to scale to large graphs or complexes.

Inspired by recent breakthroughs in selective state-space models, particularly the Mamba [Dao and Gu, 2024; Sieber *et al.*, 2024], we investigate their integration into topological deep learning. While Mamba models capture long-range dependencies efficiently in temporal sequences, they cannot be directly applied to CCs, as the multi-rank, structured topology of CCs differs fundamentally from time series. Although replacing transformers with Mamba might reduce quadratic complexity, this alone does not address the core challenges of rank-aware message propagation in CCs. Motivated by these limitations, we pose the following question: How can we rethink the state-space model to model higher-order graph structural relationships, moving beyond local aggregations to a global, sequence-aware perspective for CCs?

To address these limitations, we propose Combinatorial Complex Mamba (CCMamba), the first unified Mamba-based neural architecture for combinatorial complexes. CCMamba introduces a bidirectional, rank-aware state-space module that encodes higher-order incidence relations of CCs into structured sequences, which are then processed by selective state-space models. Treating topological relations of neighborhood information as structured sequences opens the possibility of using state-space models to achieve directional and global context-aware propagation beyond the locality constraints of existing TDL-based approaches. This design facilitates efficient message passing across nodes, edges, faces, and higher-dimensional cells. Moreover, CCMamba generalizes to graphs, hypergraphs, simplicial complexes, and cellular complexes by instantiating the corresponding incidence matrices. Our main contributions are summarized as follows:

- We propose CCMamba, the first Mamba-based neural networks on combinatorial complexes to unify a higher-order message passing framework capable of graphs, hypergraphs, simplicial and cellular complexes.
- To address quadratic complexity of self-attention mechanism, CCMamba introduces a rank-structured selective state-space, which linearizes neighborhood sequences

and models long-range propagation.

- We present a theoretical analysis demonstrating that the expressivity of CCs-based Mamba message passing is bounded above by the 1-dimensional combinatorial complex Weisfeiler–Leman (1-CCWL) test.
- We conduct extensive experiments on graph, hypergraph, and simplicial benchmarks, where CCMamba achieves superior results on node and graph classification tasks.

2 Preliminaries

2.1 Combinatorial Complexes

A combinatorial complex generalizes graphs, hypergraphs, simplicial complexes, and cellular complexes into a unified algebraic-topological structure. Formally, we define as follow:

Definition 1 (Combinatorial Complex). A combinatorial complex is a triple $(\mathcal{S}, \mathcal{C}, \text{rk})$ where

- (1) \mathcal{S} is a finite set of vertices,
- (2) $\mathcal{C} \subseteq 2^{\mathcal{S}}$ is a collection of cells,
- (3) $\text{rk} : \mathcal{C} \rightarrow \mathbb{Z}_{\geq 0}$ is an order-preserving rank function such that $\sigma \subseteq \tau$, then $\text{rk}(\sigma) \leq \text{rk}(\tau)$

The elements of \mathcal{C} are called cells (i.e., group of nodes, edges). The rank of a cell $\sigma \in \mathcal{C}$ is $k : \text{rk}(\sigma)$, and we denote it as a k -cell, such as 0-cells (nodes), 1-cells (edges), and 2-cells (faces), which simplifies notation for $(\mathcal{S}, \mathcal{C}, \text{rk})$, and its dimension are the maximal rank: $\dim(\mathcal{C}) := \max_{\sigma \in \mathcal{C}} \text{rk}(\sigma)$.

To enable the representation of higher-order structures construction, we define a lifting function $f : G \rightarrow \mathcal{C}$ to introduce and elaborate on this lifting process graph data.

Definition 2 (Lifting Operation). Let \mathcal{G} be the class of graphs and let $\mathcal{H}, \mathcal{S}, \mathcal{C}$ denote the classes of hypergraphs, simplicial complexes, and cellular complexes, respectively. A lifting operation is a function

$$f : \mathcal{G} \rightarrow \mathcal{X},$$

that lifts graph $G \in \mathcal{G}$ to higher-order graph $f(G) \in \mathcal{X} = \{\mathcal{H}, \mathcal{S}, \mathcal{C}\}$ obtained from G by a prescribed construction.

2.2 Combinatorial Complex Neural Networks

Combinatorial complex neural networks (CCNNs) generalize the classical message-passing frameworks to CCs. CCNNs extend message passing beyond pairwise relationships, which define a three-stage message passing mechanism, divide the geometric structure into multiple cell message passing mechanisms, and perform intra-neighbor aggregation and inter-neighbor fusion. Formally, we define as

Combinatorial Complex Neural Networks. Let $\mathcal{N}_{\mathcal{C}}$ be a set of neighborhoods, each defines a specific relational operator on the combinatorial complex \mathcal{C} . For each cell $\sigma \in \mathcal{C}$ with rank $\text{rk}(\sigma)$ and feature representation $h_{\sigma}^l \in \mathbb{R}^{F^l}$ at layer l , the layer update of the CCNNs can be defined as:

$$h_{\sigma}^{l+1} = \phi \left(h_{\sigma}^l, \bigotimes_{\mathcal{N} \in \mathcal{N}_{\mathcal{C}}} \bigoplus_{\tau \in \mathcal{N}(\sigma)} \psi_{\mathcal{N}, \text{rk}(\sigma)}(h_{\sigma}^l, h_{\tau}^l) \right), \quad (1)$$

where \bigoplus is intra-neighborhood aggregation over all neighbors $\tau \in \mathcal{N}(\sigma)$; \bigotimes is inter-neighborhood fusion across all neighborhood $\mathcal{N} \in \mathcal{N}_{\mathcal{C}}$; $\psi_{\mathcal{N}, k}$ is a neighborhood-specific message

function; ϕ is the update function. The rank function guarantees message aggregation within each cells neighborhood of different topological ranks.

The message function $\psi_{\mathcal{N},k}$ is parameterized as:

$$\psi_{\mathcal{N},k}(h_\sigma^l, h_\tau^l) = \alpha_{\mathcal{N}}(\sigma, \tau) W_{\mathcal{N},k} [h_\sigma^l \| h_\tau^l], \quad (2)$$

where $[h_\sigma^l \| h_\tau^l]$ is the concatenation of sender and receiver features, $W_{\mathcal{N},k} \in \mathbb{R}^{F^{l+1} \times 2F^l}$ is a learnable transformation matrix, and $\alpha_{\mathcal{N}}(\sigma, \tau)$ is computed as attention mechanism [Ballester *et al.*, 2024] and [Papillon *et al.*, 2025; Gurugubelli and Chepuri, 2024] between cells information propagation. One observes that scaled dot-product attention coefficient $\alpha_{\mathcal{N},\tau}^{(h)}$ of cell features h with neighborhood type \mathcal{N} and rank $k = \text{rk}(\sigma)$ is formulated as

$$\alpha_{\mathcal{N},k} = \text{softmax} \left(\frac{\left(W_{Q,\mathcal{N},k} \tilde{h}_\sigma \right) \left(W_{K,\mathcal{N},k} \tilde{h}_\tau \right)}{\sqrt{d/H}} \right), \quad (3)$$

where H is the number of attention heads, and $W_{Q,K,V,\mathcal{N},k}^{(h)} \in \mathbb{R}^{\frac{d}{H} \times d}$ are the query, key, and value projection matrices associated with neighborhood type \mathcal{N} , rank k , and head h . However, applying attention mechanisms to graphs, especially higher-order graphs, results in a high complexity of $O(n^2)$ when calculating the attention score for all node pairs, failing to apply to large-scale real-world networks.

2.3 State Space Models

Although attention mechanism effectively captures graph neighborhood dependencies, its quadratic computational complexity imposes computational and memory bottlenecks on CCs. Recently, the state-space models [Dao and Gu, 2024; Yuan *et al.*, 2025; Nishikawa and Suzuki, 2025] have emerged as an alternative to address the transformer’s high computation while maintaining the ability to model long sequences.

State space models (SSM) are linear time-invariant systems, which maps the sequence $x(t) \in R^L$ to the embeddings $y(t) \in R^L$. SSM employs a latent state $h(t) \in R^{N \times L}$, parameter matrices $A \in R^{N \times N}$ and $B \in R^{N \times 1}$, $C \in R^{1 \times N}$, defined as

$$h'(t) = A \cdot h(t) + Bx(t), \quad y(t) = Ch(t). \quad (4)$$

Furthermore, a discrete spatial state model is proposed to solve the information transfer in deep learning.

$$h_t = \bar{A} \cdot h_{t-1} + \bar{B}x_t, \quad y(t) = Ch(t), \quad (5)$$

where $\bar{A} = \exp(\Delta A)$, and $\bar{B} = (\Delta A)^{-1}(\exp(\Delta A - I)) \cdot \Delta B$. The selective state-space mechanism of SSM dynamically and selectively propagates information, enabling its computational complexity $O(n)$ scales linearly with the sequence length.

3 Combinatorial Complex State Space Models

3.1 Neighborhood on Combinatorial Complexes.

Let $CC = (\mathcal{S}, \mathcal{C}, rk)$ denote a 2-dimensional combinatorial complex, where cells of varying dimensions interact through generalized adjacency relations beyond pairwise connections. we consider incidence-induced, rank-coupled neighborhoods derived from the lower and upper incidence matrices: $B_1 \in \mathbb{R}^{|V_0| \times |E_1|}$ encodes node–edge incidences and

$B_2 \in \mathbb{R}^{|E_1| \times |F_2|}$ represents edge–face incidences. Here, we define four neighborhood types that govern message propagation across dimensions:

- Node–Edge neighborhoods $\mathcal{N}_{0 \rightarrow 1}(e)$: the set of nodes incident to a given edge, capture the influence of 1-cells shared 0-cells.
- Edge–Node neighborhoods $\mathcal{N}_{1 \rightarrow 0}(v)$: the collection of edges incident to a node v , reflecting the 1-cells adjacent to a 0-cell.
- Edges–Face neighborhoods $\mathcal{N}_{2 \rightarrow 1}(e)$: the set of 2-cells that contain a given edge e , enabling higher-order interactions among edges via shared faces
- Face–Edge neighborhoods $\mathcal{N}_{1 \rightarrow 2}(f)$: the set of edges that bound a face f , facilitating information flow from 1-cells to their enclosing 2-cells.

To model these neighborhoods are topologically induced by the rank function of cell. we define neighbor function as

Rank-Aware Neighborhood Function. Given a cell $\sigma \in CC$, let $\mathcal{R}(\sigma) \subseteq \{0, 1, 2\}$ denote the neighborhood set of three rank types incident to σ . Denote by $h_\sigma^{(\ell)}$ the feature of σ (k -cell) at layer ℓ , and its linearly projected feature $\tilde{h}_\sigma^{(\ell)} = W_k h_\sigma^{(\ell)}$. The CCNNs with neighborhood functions writes

$$h_\sigma^{(\ell+1)} = \phi_1 \left(h_\sigma^{(\ell)}, \phi_2 \left(\phi_3 \left(h_\sigma^{(\ell)}, \{\tilde{h}_\tau^{(\ell)}\}_{\tau \in \mathcal{N}_{k \rightarrow r}(\sigma)} \right) \right)_{r \in \mathcal{R}(\sigma)} \right), \quad (6)$$

where ϕ_1, ϕ_2, ϕ_3 aggregates projected neighbor features, and $\mathcal{N}_{k \rightarrow r}(\sigma)$ is the propagate information from k -cell to r -cell, and ϕ represents a message passing neural network to aggregate information from different neighbors with ranks.

3.2 Combinatorial Complex Mamba Networks

While combinatorial complex message-passing networks enable higher-order interaction modeling, their reliance on attention-based neighborhood fusion incurs quadratic complexity and struggles to model long-range dependencies. To address this, we propose Combinatorial Complex Mamba in Figure 2, a novel framework that integrates selective state-space models into the topological message-passing process.

Mamba Block Message Passing Layer Each Mamba block is formulated as a learnable linear-time recurrent filter based on a selective state-space model (SSM), the state transition dynamics are explicitly conditioned on the input features. For each rank k at layer ℓ , the SSM computes its representation $h_{\text{intra},k}^{(\ell)}$ via the following parameterization:

$$\begin{aligned} A_k &= -\exp(W_{A,k} h_k^{(\ell)} + b_{A,k}), B_k = W_{B,k} h_k^{(\ell)}, \\ C_k &= W_{C,k} h_k^{(\ell)}, \Delta_k = \text{Softplus}(W_{\Delta,k} h_k^{(\ell)} + b_{\Delta,k}), \\ y_k &= \text{SSM}_{\text{selective}}(A_k, B_k, C_k, \Delta_k, k_k^{(\ell)}), \\ z_k &= \sigma(W_{z,k} h_k^{(\ell)}), h_{\text{intra},k}^{(\ell)} = W_{\text{out},k}(z_k \odot y_k), \end{aligned} \quad (7)$$

where A_k , B_k , and C_k respectively parameterize the state transition, input injection, and readout operators of the SSM, while Δ_k controls the discretization step size and thereby

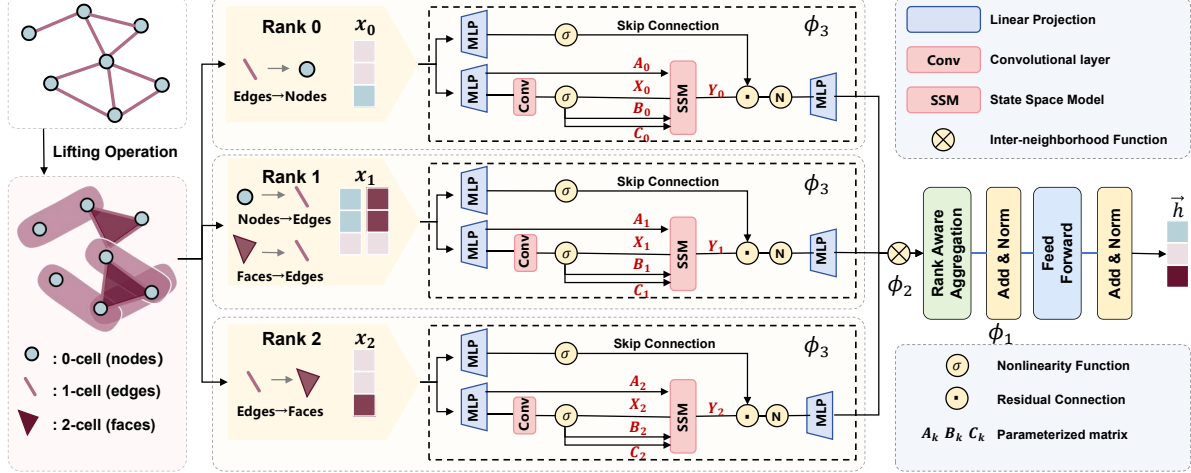


Figure 2: The framework of our proposed Combinatorial Complex Mamba method.

the effective temporal scale of the dynamics. Softplus is the activation function defined as $\text{Softplus}(x) = \ln(1 + e^x)$. The negative exponential in A_k enforces strictly negative transition coefficients, which guarantees the stability of the continuous-to-discrete state evolution. The gating vector z_k modulates the SSM output through element-wise multiplication before the final linear projection $W_{\text{out},k}$. This formulation yields stable propagation dynamics for each rank, with linear-time complexity in the number of cells.

Intra-neighborhood Message Passing via SSM. Each layer updates the rank-specific features $(h_0^{(\ell)}, h_1^{(\ell)}, h_2^{(\ell)})$ for nodes, edges, and faces, respectively. Let $B_1 \in \mathbb{R}^{|V_0| \times |E_1|}$ and $B_2 \in \mathbb{R}^{|E_1| \times |V_2|}$ be node–edge and edge–face incidence matrices, respectively. Leveraging these operators, the function ϕ_3 of CCMamba update features at layer ℓ can be computed as

$$\begin{aligned} h_{\text{intra},0}^{(\ell+1)} &= \text{MLP}_0^{(\ell)} \left(\text{Mamba}_0^{(\ell)} \left(W_0^{(\ell)} [h_0^{(\ell)}, B_1, h_1^{(\ell)}] \right) \right), \\ h_{\text{intra},1}^{(\ell+1)} &= \text{MLP}_1^{(\ell)} \left(\text{Mamba}_1^{(\ell)} \left(W_1^{(\ell)} [h_1^{(\ell)}, B_1^\top h_0^{(\ell)}, B_2, h_2^{(\ell)}] \right) \right), \\ h_{\text{intra},2}^{(\ell+1)} &= \text{MLP}_2^{(\ell)} \left(\text{Mamba}_2^{(\ell)} \left(W_2^{(\ell)} [h_2^{(\ell)}, B_2^\top h_1^{(\ell)}] \right) \right), \end{aligned} \quad (8)$$

where $W_k^{(\ell)}(\cdot)$ and $\text{MLP}_k^{(\ell)}(\cdot)$ are rank-specific linear projections that align feature dimensions before and after the Mamba blocks. Each Mamba_k filters its input sequence to produce rank-aware representations. This update design implements three coupled message flows: (1) node–node interactions mediated through shared edges ($B_1 x_1$), (2) edge–edge interactions through shared nodes and faces ($B_1^\top x_0, B_2 x_2$), and (3) face–edge interactions via boundary relations ($B_2^\top x_1$).

Inter-neighborhood Rank-Level Aggregation. Following the rank-wise selective state-space propagation in Equation 8, CCMamba aggregates information across different topological ranks to generate contextually enriched embeddings for each cell. Specifically, for a cell σ , $\mathcal{R}(\sigma)$ denotes the set of ranks adjacent to σ via incidence relations (e.g., a edge is adjacent to nodes and faces). Let $\mathbf{h}_{\text{intra},\sigma}^{(\ell)}$ be the representation of σ after

intra-rank propagation, and $\tilde{\mathbf{H}}_{\text{intra},\mathcal{N}_r(\sigma)}^{(\ell)}$ denote the collection of neighbor representations $h_{\text{intra},r}^{(\ell)}$ at rank r . For k -cell, the embedding function ϕ_2 at layer $\ell + 1$ is computed with the summation function, defined as

$$h_k^{(\ell+1)} = \phi_1 \left(\mathbf{h}_k^{(\ell)}, \text{MLP} \left(\sum_{r \in \mathcal{R}(\sigma)} (\tilde{\mathbf{h}}_r^{(\ell)}, \tilde{\mathbf{H}}_{\text{intra},\mathcal{N}_r(\sigma)}^{(\ell)}) \right) \right), \quad (9)$$

where ϕ_1 is a nonlinear update function (e.g., an MLP), and Mamba_r denotes the rank-specific selective state-space module that dynamically filters and integrates cross-rank contextual signals. This construction provides a unified state-space interpretation of higher-order message passing while remaining faithful to the combinatorial structure of the complex.

After computing rank-wise outputs $h_{\text{intra},0}^{(\ell+1)}, h_{\text{intra},1}^{(\ell+1)}, h_{\text{intra},2}^{(\ell+1)}$, the CCMamba layer refines each representation through residual connections, dropout, and layer normalization:

$$\begin{aligned} \hat{h}_k^{(\ell+1)} &= \text{LayerNorm} (h_k^{(\ell+1)} + \text{Dropout}(h_{\text{intra},k}^{(\ell+1)})), \\ h_k^{(\ell+1)} &= \text{LayerNorm} (\hat{h}_k^{(\ell+1)} + \text{FFN}(\hat{h}_k^{(\ell+1)})), \end{aligned} \quad (10)$$

where each rank $k \in \{0, 1, 2\}$ (nodes, edges, faces). This post-processing preserves the incidence-aware structure learned in Equations 1 and 9, while stabilizing training through residual learning. The cell embeddings $\{h_k^{(L)}\}_{k=0,1,2}$ at the final layer L are then pooled to produce representations for downstream tasks such as node classification or graph-level prediction.

4 How Powerful are CCMamba?

The expressive power of message-passing graph neural networks is fundamentally limited by the Weisfeiler–Lehman (WL) hierarchy: standard GNNs are at most as powerful as the 1-WL test [Xu *et al.*, 2018], while hypergraph GNNs often fail to exceed this bound due to their reliance on symmetric neighborhood aggregation. In contrast, combinatorial complexes support richer incidence structures that enable more refined

topological discrimination. This raises a natural question: How expressive is CCMamba in representing combinatorial complexes? To fill this gap, we analyze the CCMamba layer through the Weisfeiler–Lehman test with rank-aware cell designed for combinatorial complexes state space models.

4.1 Generalized Weisfeiler–Lehman Algorithm

Definition 3 (Labeled Combinatorial Complex). A labeled combinatorial complex (C, ℓ) is a CC equipped with a cell coloring $\ell : C \rightarrow \mathbb{N}$. We define $\ell(\sigma)$ is the label coloring of a cell $\sigma \in C$ on combinatorial complex.

Definition 4 (Combinatorial Complex Weisfeiler–Lehman (CCWL)). Given a $CC(\mathcal{S}, \mathcal{C}, rk, \ell^v, \ell^e, \ell^f)$ and a function $r : (\mathcal{S}, \mathcal{C}, rk, l_i^v, l_i^e, l_i^f) \rightarrow (\mathcal{S}, \mathcal{C}, rk, l_{i+1}^v, l_{i+1}^e, l_{i+1}^f)$, here r is colorings relabel function. we denote by CC_i the relabeled combinatorial complex after i iterations. Then the Combinatorial Complex WL sequence is defined as

$$\{CC^{(0)}, \dots, CC^{(h)}\} = \{(\mathcal{S}, \mathcal{C}, rk, \ell_v^{(i)}, \ell_e^{(i)}, \ell_f^{(i)})\}_{i=0}^h$$

where $CC^0 = CC$ and $\ell_0 = (\ell_v^{(0)}, \ell_e^{(0)}, \ell_f^{(0)})$.

CCWL test employs by labeling the vertices, edges and faces with $\ell_v^{(0)}, \ell_e^{(0)}, \ell_f^{(0)} = 0$. For iteration $k = 0, \dots, h-1$, $\ell^{(k+1)}$ are relabeled with the k -th labels $\ell^{(k)}$ on edge, face and nodes, respectively. The new labels are updated as

$$\begin{aligned} \ell_v^{(k+1)} &= \{\{\ell_v^{(k)}, \{\ell_e^{(k)}\}_{e \in E_v}\}\}, \\ \ell_e^{(k+1)} &= \{\{\ell_e^{(k)}, \{\ell_v^{(k)}\}_{v \in V_e}, \{\ell_f^{(k)}\}_{f \in F_e}\}\}, \\ \ell_f^{(k+1)} &= \{\{\ell_f^{(k)}, \{\ell_e^{(k)}\}_{e \in E_f}\}\}, \end{aligned} \quad (11)$$

where E_v, V_e, F_e, E_f are the edges connected to nodes, nodes connected to edges, faces connected to edges and edges connected faces, respectively. $\{\{\}\}$ denotes a multiset.

1-CCWL distinguish CC_1 and CC_2 as non-isomorphic if there exists a cell at k -iteration such that the condition

$$\{\{l_{CC_1, \sigma_1}^{(k)} | \sigma_1 \in CC_1\}\} \neq \{\{l_{CC_2, \sigma_2}^{(k)} | \sigma_2 \in CC_2\}\}, \quad (12)$$

then we can conclude that

Proposition 1 (1-CCWL). If 1-CCWL test decides CC_1 and CC_2 are non-isomorphic, then $CC_1 \neq CC_2$.

Suppose the same features to all cells in combinatorial which allows CCMamba to rely only on the structure to learn. Let $\mathcal{A} : CC \rightarrow R^d$ be a CCMamba Layer in Equation 1, we can conclude the Lemma as

Lemma 1. Suppose an injective function $\mathcal{A} : CC_1 \rightarrow CC_2$, and let the labels $\ell_{CC}^{(k)} = \{\ell_v^{(k)}, \ell_e^{(k)}, \ell_f^{(k)}\}$, and features $h_{CC}^{(k)} = \{h_v^{(k)}, h_e^{(k)}, h_f^{(k)}\}$ of node, edge and face in combinatorial complex CC at iteration k , respectively. If the conditions hold,

$$\begin{cases} l_{CC_1, \sigma_1}^{(j)} = l_{CC_2, \sigma_2}^{(j)}, & \forall j \leq k \\ h_{CC_1, \sigma_1}^{(j)} = h_{CC_2, \sigma_2}^{(j)}, & \forall j \leq k-1 \end{cases} \quad (13)$$

for iterations $0, 1, \dots, k$. Then, for the condition in Equation 14 holds, it follows that $h_{CC_1, \sigma_1}^{(k)} = h_{CC_2, \sigma_2}^{(k)}$ at iterations k .

We conclude that the upper bounded of CCMamba layer \mathcal{A} 's expressive power is 1-CCWL test.

Proposition 2. Given two non-isomorphic combinatorial complexes CC_1 and CC_2 , if \mathcal{A} can distinguish them by $\mathcal{A}(CC_1) \neq \mathcal{A}(CC_2)$, then 1-CCWL test also decides $CC_1 \neq CC_2$.

Theorem 1. Given two non-isomorphic combinatorial complexes CC_1 and CC_2 , a CCMamba Layer \mathcal{A} can distinguish them, if conditions hold. Under the conditions of Lemma 2 and with an injective permutation-invariant readout

1. Local Level. ϕ_1, ϕ_2 functions are injective.
2. Global Level. In addition to the local-level conditions, \mathcal{A} 's graph-level READOUT function is injective.

All proofs are in the Supplementary Material Section C.

5 Experiments

In this section, we evaluate the performance of the proposed framework CCMamba in extensive experiments.

Datasets We evaluate CCMamba on the real-world benchmarks. For graph classification, we use standard TUDatasets [Morris *et al.*, 2020], including: molecular graphs (MUTAG, PROTEINS) for chemical property and protein function prediction; social networks (IMDB-BINARY, IMDB-MULTI); and heterophilic graphs from the HeterophilicGraph-Dataset [Platonov *et al.*, 2023], namely AMAZON-RATINGS, ROMAN-EMPIRE, and MINESWEEPER. At the node classification level, we adopt the citation networks Cora, CiteSeer, and PubMed [Yang *et al.*, 2016]. Following the structural lifting methods provided by TOPOBENCH [Telyatnikov *et al.*, 2024], we lift all base graphs into higher-order structures, such as hypergraphs, simplicial complexes, and cellular complexes. Details are provided in Supplementary Material Section B.

Baselines Models We compare against a broad range of baselines spanning multiple topological domains: Graph neural networks: GCN [Kipf, 2016], GAT [Vaswani *et al.*, 2017], GIN [Xu *et al.*, 2018]. Hypergraph neural networks: HyperGCN [Yadati *et al.*, 2019], HyperGAT [Ding *et al.*, 2020], UniGCN, UniGNNII and UniSAGE [Huang and Yang, 2021], AllSet [Chien *et al.*, 2021], EDGNN [Jo *et al.*, 2021]. Simplicial complex networks: SCCN and SCCNN [Yang *et al.*, 2022], SGAT [Lee *et al.*, 2022] SCN [Roddenberry *et al.*, 2021; Lecha *et al.*, 2025], SANN [Gurugubelli and Chepuri, 2024]. Cellular complexes networks: CCNN, CXN [Hajij *et al.*, 2020], CWN [Bodnar *et al.*, 2021], CCCN [Papillon *et al.*, 2025]. All models are evaluated on the same lifted higher-order representations (hypergraphs, simplicial complexes, or cellular complexes) to ensure a fair comparison.

5.1 Graph Classification and Node Classification

We evaluate the proposed CCMamba framework on both graph-level and node-level classification tasks, which require leveraging high-order relational structures—such as hypergraphs, simplicial complexes, and cellular complexes. All competing methods are trained under identical hyperparameter configurations to ensure a fair comparison. We instantiate CCMamba under four topological instantiations, including CCMamba(graph), CCMamba(hypergraph), CCMamba(simplicy), and CCMamba(rank-cell).

	Model	Graph Level Tasks						Node Level Tasks			Mean	
		MUTAG	PROTEINS	IMDB-B	IMDB-M	ROMAN-E	AMAZON-R	Minesweeper	Cora	Citeseer	PubMed	
Graph	GCN	70.21 \pm 2.43	72.76 \pm 1.78	70.80 \pm 2.04	49.33 \pm 4.52	78.10 \pm 1.15	49.84 \pm 3.71	83.48 \pm 0.69	87.00 \pm 2.11	75.51 \pm 3.47	89.48 \pm 1.29	72.65
	GAT	72.34 \pm 1.69	74.91 \pm 2.34	68.40 \pm 3.73	46.93 \pm 4.25	83.25 \pm 1.82	49.29 \pm 3.94	83.84 \pm 1.01	86.71 \pm 2.25	73.59 \pm 3.77	89.21 \pm 1.25	72.75
	GIN	78.72 \pm 2.61	76.70 \pm 1.87	71.20 \pm 1.86	46.40 \pm 4.07	79.92 \pm 2.20	49.22 \pm 3.58	83.60 \pm 0.37	87.59 \pm 1.92	73.11 \pm 4.08	89.51 \pm 0.94	73.18
Hypergraph	HperGCN	75.53 \pm 2.05	73.82 \pm 2.17	67.60 \pm 2.38	45.87 \pm 4.18	76.40 \pm 1.92	48.91 \pm 3.66	80.24 \pm 1.27	86.35 \pm 4.26	72.41 \pm 2.04	88.35 \pm 0.97	71.55
	UniGCN	72.34 \pm 2.28	75.27 \pm 2.06	69.20 \pm 3.67	47.20 \pm 3.93	75.80 \pm 2.17	47.46 \pm 4.16	80.68 \pm 1.63	87.44 \pm 2.38	71.31 \pm 4.33	85.15 \pm 2.60	71.19
	HyperGAT	68.51 \pm 12.04	70.25 \pm 2.08	70.08 \pm 2.38	34.67 \pm 2.08	71.56 \pm 0.39	48.11 \pm 0.16	79.82 \pm 0.49	85.05 \pm 1.03	72.45 \pm 1.83	82.87 \pm 0.39	68.34
	UniGNII	82.98 \pm 1.46	73.48 \pm 2.68	71.20 \pm 2.03	47.20 \pm 3.72	73.00 \pm 2.98	48.75 \pm 3.50	80.72 \pm 1.55	87.59 \pm 1.73	74.79 \pm 3.08	88.59 \pm 0.77	72.93
	UniGIN	79.23 \pm 4.81	71.26 \pm 2.09	68.48 \pm 2.17	32.69 \pm 1.06	73.29 \pm 0.28	48.75 \pm 0.43	80.36 \pm 0.79	84.64 \pm 0.78	72.53 \pm 1.09	83.08 \pm 0.41	69.43
	UniSAGE	78.72 \pm 1.43	74.55 \pm 3.76	71.60 \pm 4.72	34.67 \pm 2.74	74.53 \pm 3.81	49.70 \pm 0.48	80.85 \pm 0.62	85.55 \pm 0.76	73.78 \pm 1.39	83.08 \pm 0.41	70.70
	AllSet	74.47 \pm 2.55	76.70 \pm 1.97	64.40 \pm 2.92	47.47 \pm 3.81	77.52 \pm 2.38	50.02 \pm 3.27	81.88 \pm 1.49	83.60 \pm 2.83	74.31 \pm 3.29	89.05 \pm 1.75	71.94
	EdGNN	80.85 \pm 1.63	74.91 \pm 2.26	70.40 \pm 2.48	49.53 \pm 4.15	79.99 \pm 1.78	48.38 \pm 3.85	83.12 \pm 0.99	84.44 \pm 2.04	75.03 \pm 3.19	89.39 \pm 1.15	73.60
Simplex	SCCN	76.60 \pm 2.06	75.63 \pm 1.88	69.60 \pm 2.84	48.20 \pm 3.43	83.06 \pm 1.07	50.15 \pm 3.49	83.92 \pm 0.75	81.24 \pm 3.57	69.03 \pm 4.55	87.85 \pm 1.92	72.53
	SAN	71.38 \pm 5.73	71.54 \pm 2.20	64.45 \pm 4.27	45.35 \pm 2.83	84.70 \pm 2.79	48.99 \pm 3.41	82.84 \pm 2.41	66.23 \pm 0.71	62.50 \pm 0.94	88.74 \pm 2.69	68.65
	SCCNN	70.21 \pm 2.82	75.63 \pm 1.97	69.20 \pm 3.04	47.73 \pm 3.58	84.69 \pm 0.98	50.33 \pm 2.91	83.36 \pm 0.86	82.13 \pm 3.23	70.59 \pm 4.28	87.83 \pm 2.08	72.17
	SCN	72.34 \pm 2.55	75.60 \pm 2.07	68.80 \pm 2.74	47.00 \pm 3.82	84.16 \pm 1.13	49.88 \pm 3.23	85.44 \pm 0.68	81.39 \pm 0.39	71.91 \pm 4.17	88.70 \pm 1.62	72.60
	SANN	74.29 \pm 1.63	77.62 \pm 2.28	72.7 \pm 2.16	48.97 \pm 1.02	84.01 \pm 2.06	51.34 \pm 1.72	84.73 \pm 0.93	82.46 \pm 2.79	73.19 \pm 2.11	87.26 \pm 0.98	73.66
Cellular	CCNN	74.47 \pm 2.17	72.04 \pm 2.76	72.00 \pm 1.92	49.33 \pm 3.27	81.54 \pm 1.33	51.07 \pm 2.97	84.08 \pm 0.83	87.44 \pm 2.28	74.07 \pm 3.32	88.09 \pm 2.15	73.41
	CCXN	76.60 \pm 1.92	73.48 \pm 2.57	70.80 \pm 2.37	46.93 \pm 3.83	81.15 \pm 1.46	48.24 \pm 3.69	83.28 \pm 1.08	87.30 \pm 2.44	73.95 \pm 3.63	88.34 \pm 1.87	73.01
	CWN	82.47 \pm 1.34	74.19 \pm 2.27	72.40 \pm 2.17	49.07 \pm 3.42	82.55 \pm 1.27	50.99 \pm 3.14	84.00 \pm 0.73	85.23 \pm 2.77	73.47 \pm 3.83	87.44 \pm 2.37	74.18
	CCCN	76.60 \pm 2.02	73.48 \pm 2.47	70.00 \pm 2.56	48.00 \pm 3.63	82.28 \pm 1.51	50.48 \pm 3.37	85.36 \pm 0.73	87.44 \pm 1.96	74.31 \pm 3.42	88.58 \pm 1.73	73.65
Ours	CCMamba(graph)	79.75 \pm 2.40	77.42 \pm 4.10	73.20 \pm 3.50	52.80\pm3.70	83.46 \pm 2.40	52.92\pm2.85	85.52\pm1.10	88.12 \pm 0.93	76.11 \pm 2.60	89.51 \pm 1.87	75.88
	CCMamba(hypergraph)	78.72 \pm 2.10	76.67 \pm 2.30	72.40 \pm 2.60	46.40 \pm 3.90	78.52 \pm 1.80	49.53 \pm 2.23	83.48 \pm 1.05	87.59 \pm 3.16	75.03 \pm 4.16	89.53\pm2.63	73.79
	CCMamba(simplex)	76.60 \pm 2.48	69.18 \pm 3.15	71.20 \pm 2.91	42.27 \pm 4.28	85.51\pm1.24	48.90 \pm 3.53	81.12 \pm 1.82	70.71 \pm 1.56	73.27 \pm 2.63	87.61 \pm 2.75	70.64
	CCMamba(rank-cell)	85.11\pm2.40	78.14\pm1.68	74.81\pm1.85	50.13 \pm 3.02	85.49 \pm 1.72	50.34 \pm 2.74	84.57 \pm 3.10	89.22\pm1.50	76.95\pm2.90	89.29 \pm 1.47	76.41

Table 1: Test accuracy (%) of CCMamba and baseline methods across graph classification and node classification on citation networks. Highest and second-highest scores per dataset can be highlighted in **bold** and underlined, respectively.

CCMamba vs. Baselines. Table 1 shows that CCMamba (rank-cell) achieves state-of-the-art or near state-of-the-art performance on several established graph classification benchmarks. This confirms that the state-space-based message-passing mechanism effectively captures structural patterns on standard graph structures. Moreover, CCMamba(rank-cell) demonstrates superior performance on datasets characterized by intricate higher-order interactions (e.g., 85.11% on MUTAG and 78.14% on PROTEINS). It also yields the highest average accuracy across the evaluated graph classification tasks. For node classification, CCMamba exhibits consistent and competitive results across different topological abstractions. Notably, CCMamba (rank-cell) achieves 89.22% accuracy on Cora and 76.95% on Citeseer. This improvement suggests that incorporating rank-aware cellular relations enables more expressive propagation of information through complex, non-pairwise neighborhoods. These results validate CCMamba as a unified, topology-agnostic message-passing architecture grounded in state-space modeling, capable of generalizing across diverse structures with notable performance.

CCMamba vs. Attention. Table 2 reports the comparison between attention-based aggregation (GAT and MultiGAT) and selective state-space aggregation (CCMamba and MultiCCMamba) across node-level and graph-level tasks. All methods share the same backbone architecture, differing only in the message aggregation mechanism. Mamba-based models outperform their attention-based counterparts across most datasets and structural settings. On node classification tasks, CCMamba and MultiCCMamba achieve the higher accuracy under graph, simplicial, and cellular representations with considerable gains (e.g., CCMamba(simplex) vs. GAT +19.5% on Cora, MultiCCMamba(graph) vs. MultiGAT +6.5%). Similar

trends are observed for graph-level tasks. Mamba-based variants attain superior performance (e.g., CCMamaba(graph) vs. GAT: +5.9% on MUTAG, CCMamaba(hypergraph) +48.9% on IMDB-M). Overall, MultiCCMamba consistently improves over MultiGAT, indicating that the observed gains stem from the aggregation mechanism rather than increased model capacity under higher-order topological representations.

	Dataset	Structure	GAT	CCMamba	MultiGAT	MultiCCMamba
Node Level Tasks	Cora	Graph	86.71 \pm 2.50	88.12 \pm 0.93	86.26 \pm 0.79	89.78\pm3.21
		Hypergraph	85.05 \pm 1.03	75.92 \pm 2.67	86.35 \pm 1.37	89.51\pm3.22
		Simplex	66.23 \pm 0.71	79.17 \pm 1.38	69.51 \pm 1.37	79.35\pm0.89
		Cellular	86.71 \pm 2.36	<u>89.07\pm4.77</u>	88.47 \pm 3.61	89.52\pm2.19
Graph Level Tasks	Citeseer	Graph	73.59 \pm 3.7	76.51 \pm 2.90	75.87 \pm 1.80	77.43\pm1.50
		Hypergraph	72.45 \pm 1.83	74.55 \pm 1.55	73.71 \pm 1.18	77.43\pm3.02
		Simplex	62.50 \pm 0.94	64.33 \pm 1.89	65.27 \pm 7.50	69.51\pm8.19
		Cellular	74.97 \pm 4.17	75.51 \pm 1.93	<u>76.35\pm2.18</u>	77.31\pm4.03
Node Level Tasks	Pubmed	Graph	88.38 \pm 0.28	89.51 \pm 1.87	89.14 \pm 2.51	89.86\pm0.41
		Hypergraph	82.85 \pm 0.40	87.89 \pm 3.05	87.47 \pm 2.97	88.37\pm2.51
		Simplex	62.50 \pm 0.94	78.82 \pm 2.95	79.39 \pm 3.16	87.36\pm4.01
		Cellular	88.21 \pm 5.27	89.29 \pm 1.63	89.46\pm3.68	89.39 \pm 3.91
Graph Level Tasks	IMDB-M	Graph	72.34 \pm 1.93	76.60 \pm 2.4	73.49 \pm 5.23	78.72\pm4.86
		Hypergraph	68.72 \pm 12.34	72.34 \pm 5.00	73.77 \pm 5.63	74.28\pm1.05
		Simplex	66.89 \pm 9.70	73.94 \pm 8.20	68.08 \pm 10.53	74.47\pm8.16
		Cellular	70.21 \pm 6.03	<u>74.47\pm4.84</u>	71.64 \pm 2.83	76.60\pm1.49
Node Level Tasks	PROTEINS	Graph	48.21 \pm 3.35	52.80\pm3.78	49.91 \pm 2.57	51.20 \pm 3.17
		Hypergraph	34.19 \pm 1.93	50.93 \pm 1.47	44.93 \pm 2.84	51.98\pm0.84
		Simplex	35.27 \pm 2.01	37.60 \pm 2.64	35.91 \pm 2.56	39.62\pm3.71
		Cellular	48.92 \pm 2.71	<u>51.73\pm2.83</u>	50.13 \pm 2.48	53.40\pm1.53

Table 2: Test accuracy (%) of GAT, Mamba, MultiGAT, and MultiCCMamba on node-level and graph-level tasks.

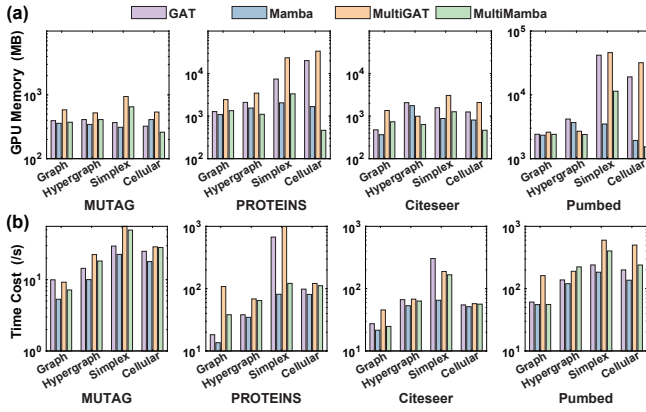


Figure 3: Comparison of GPU Memory (MB) and Time Cost(s).

Efficiency Analysis. CCMamba also exhibits substantially improved computational efficiency. As illustrated in Figure 3, the selective state-space formulation enables linear-time message propagation with respect to the number of cells. For instance, on the PROTEINS dataset with simplex structures, MultiCCMamba reduces training time from 1265.9s to 121.3s (+ 90.4% reduction), and GPU from 23518MB to 3342MB (+85.8%) compared to MultiGAT. This allows CCMamba to scale to larger complexes and higher-order neighborhoods, making it well suited for both node-level and graph-level learning on high-order topological data. These results position CCMamba as a scalable and effective alternative to higher-order graph attention mechanisms for structured data.

5.2 Expressive Power of CCMamba

To evaluate the expressive power of CCMamba(GIN), we compare it with isomorphism-based neural networks on different combinatorial structures, including GIN (graph), UniGIN (hypergraph), and CWN (cellular). As illustrated in Table 3, CCMamba(GIN) consistently achieves comparable or superior performance across both graph-level and node-level benchmarks requiring richer structural discrimination. For instance, on IMDB-M, CCMamba(GIN) improves over GIN (e.g., 51.27% vs. 46.40%, +4.57%). This empirical evidence aligns with our theoretical analysis and confirms that theoretical soundness of CCMamba and indicate that its expressive power bound reaches 1-CCWL test.

5.3 Deep-layered CCMamba Analysis

Table 4 reports the performance of CCMamba as layer depth increases to evaluate its robustness against over-smoothing. GCN and higher-order graph-based convolutional models (HyperGCN, SCCN, CCCN) suffer severe performance degradation as depth grows, often collapsing beyond a small number of layers. For instance, on Cora, HyperGCN drops sharply from 84.34% at 2 layers to around 12% at 8 layers. In contrast, CCMamba remains stable across a wide range of depths, exhibiting only marginal performance decay even with deep architectures. On Cora, CCMamba(graph) maintains accuracy from 2 to 32 layers (87.44% vs. 87.74%). By leveraging selective state-space aggregation instead of repeated local averaging, CCMamba preserves discriminative information over

deeper-layers, thereby mitigating over-smoothing problem.

Dataset	GIN	UniGIN	CWN	CCMamba(GIN)
MUTAG	78.72 ± 2.61	79.23 ± 4.85	82.47 ± 1.34	78.88 ± 3.75
PROTEINS	76.70 ± 1.87	71.26 ± 2.09	74.19 ± 2.27	77.42 ± 2.71
IMDB-B	71.20 ± 1.86	68.48 ± 2.17	72.20 ± 2.17	72.40 ± 2.31
IMDB-M	46.40 ± 4.07	32.69 ± 1.06	49.07 ± 3.42	51.27 ± 3.03
ROMAN-E	79.92 ± 2.20	73.29 ± 0.28	82.55 ± 1.27	87.12 ± 0.99
AMAZON-R	49.22 ± 3.58	48.75 ± 0.43	50.99 ± 3.14	50.08 ± 1.28
Minesweeper	83.60 ± 0.37	80.36 ± 0.79	84.00 ± 0.73	84.88 ± 0.93
Cora	87.59 ± 1.92	84.64 ± 0.78	85.23 ± 2.77	88.53 ± 1.39
Citeseer	73.11 ± 4.08	72.53 ± 1.09	73.47 ± 3.83	77.07 ± 3.26
PubMed	89.51 ± 0.94	83.08 ± 0.41	87.44 ± 2.37	89.61 ± 1.48

Table 3: Testing accuracies (%) of GIN, UniGIN, CWN and CCMamba on various graph benchmarks (mean \pm std).

Datasets	Models	Layers					
		2	4	8	16	32	64
Cora	GCN	87.00	85.23	82.27	79.24	74.43	73.26
	HyperGCN	84.34	79.62	12.70	12.38	12.85	13.29
	SCCN	71.34	68.83	54.51	47.27	41.65	55.69
	CCCN	88.18	86.56	84.34	82.57	77.84	74.30
Citeseer	CCMamba(graph)	87.44	88.77	87.89	88.04	87.74	78.07
	CCMamba(hypergraph)	88.92	88.48	85.52	76.96	76.51	77.40
	CCMamba(simplex)	86.51	84.50	75.48	73.26	73.56	74.13
	CCMamba(rank-cell)	89.07	88.33	86.07	76.66	77.40	76.07
Pubmed	GCN	75.75	73.59	70.47	69.75	69.15	67.83
	HyperGCN	72.75	70.71	8.40	7.44	8.40	7.68
	SCCN	66.39	64.95	62.91	45.86	39.86	54.26
	CCCN	76.23	72.75	70.11	68.79	68.91	68.55
	CCMamba(graph)	76.11	77.43	76.47	74.43	74.31	72.63
	CCMamba(hypergraph)	76.95	75.99	76.23	73.59	74.79	74.07
	CCMamba(simplex)	67.23	69.27	72.15	70.83	71.43	68.79
	CCMamba(rank-cell)	76.51	74.91	73.59	73.47	72.87	73.62

Table 4: Testing accuracies(%) of multiple CCMamba variants with different layer depths (2,4,8,16,32,64) in node classification task.

6 Conclusion

This paper proposes Combinatorial Complex Mamba (CCMamba), which reformulates message passing on combinatorial complexes from a state-space modeling perspective. In contrast to existing TDL methods that rely on attention-based aggregation and suffer from quadratic complexity, CCMamba provides an efficient and expressive alternative. By enabling rank-aware and long-range information propagation with linear complexity, CCMamba generalizes across graphs, hypergraphs, simplicial complexes, and cellular complexes, while achieving expressive power characterized by the 1-CCWL test. Moreover, CCMamba displays strong robustness to depth, effectively mitigating over-smoothing problem. Overall, our results on real-data benchmarks indicate that structured state-space models constitute a scalable and principled foundation for higher-order representation learning beyond graphs.

Ethical Statement

There are no ethical issues.

Supplementary Material

Related works, dataset details, baseline methods, extended experimental results, detailed proofs, additional and source code are available in the supplementary material submitted with this manuscript.

References

[Ballester *et al.*, 2024] Rubén Ballester, Pablo Hernández-García, Mathilde Papillon, Claudio Battiloro, Nina Miolane, Tolga Birdal, Carles Casacuberta, Sergio Escalera, and Mustafa Hajij. Attending to topological spaces: The cellular transformer. *arXiv preprint arXiv:2405.14094*, 2024.

[Battiloro *et al.*, 2024] Claudio Battiloro, Indro Spinelli, Lev Telyatnikov, Michael M Bronstein, Simone Scardapane, and Paolo Di Lorenzo. From latent graph to latent topology inference: Differentiable cell complex module. In *The Twelfth International Conference on Learning Representations*, 2024.

[Behrouz and Hashemi, 2024] Ali Behrouz and Farnoosh Hashemi. Graph mamba: Towards learning on graphs with state space models. In *Proceedings of the 30th ACM SIGKDD conference on knowledge discovery and data mining*, pages 119–130, 2024.

[Bick *et al.*, 2024] Aviv Bick, Kevin Li, Eric Xing, J Zico Kolter, and Albert Gu. Transformers to ssms: Distilling quadratic knowledge to subquadratic models. *NeurIPS*, 37:31788–31812, 2024.

[Bodnar *et al.*, 2021] Cristian Bodnar, Fabrizio Frasca, Nina Otter, Yuguang Wang, Pietro Lio, Guido F Montufar, and Michael Bronstein. Weisfeiler and lehman go cellular: Cw networks. *NeurIPS*, 34:2625–2640, 2021.

[Bodnar, 2023] Cristian Bodnar. *Topological deep learning: graphs, complexes, sheaves*. PhD thesis, Cambridge, UK, 2023.

[Cai *et al.*, 2022] Derun Cai, Moxian Song, Chenxi Sun, Baofeng Zhang, Shenda Hong, and Hongyan Li. Hypergraph structure learning for hypergraph neural networks. In *International Joint Conference on Artificial Intelligence*, pages 1923–1929, 2022.

[Chien *et al.*, 2021] Eli Chien, Chao Pan, Jianhao Peng, and Olgica Milenkovic. You are allset: A multiset function framework for hypergraph neural networks. In *International Conference on Learning Representations*, 2021.

[Dao and Gu, 2024] Tri Dao and Albert Gu. Transformers are ssms: Generalized models and efficient algorithms through structured state space duality. In *Forty-first International Conference on Machine Learning*, 2024.

[Ding *et al.*, 2020] Kaize Ding, Jianling Wang, Jundong Li, Dingcheng Li, and Huan Liu. Be more with less: Hypergraph attention networks for inductive text classification. In *Proceedings of the 2020 Conference on Empirical Methods in Natural Language Processing (EMNLP)*, pages 4927–4936, 2020.

[Ding *et al.*, 2023] Kaize Ding, Albert Jiongqian Liang, Bryan Perozzi, Ting Chen, Ruoxi Wang, Lichan Hong, Ed H Chi, Huan Liu, and Derek Zhiyuan Cheng. Hyperformer: Learning expressive sparse feature representations via hypergraph transformer. In *Proceedings of the 46th international ACM SIGIR conference on research and development in information retrieval*, pages 2062–2066, 2023.

[Feng *et al.*, 2019] Yifan Feng, Haoxuan You, Zizhao Zhang, Rongrong Ji, and Yue Gao. Hypergraph neural networks. In *Proceedings of the AAAI conference on artificial intelligence*, volume 33, pages 3558–3565, 2019.

[Gurugubelli and Chepuri, 2024] Sravanthi Gurugubelli and Sundeep Prabhakar Chepuri. Sann: Simple yet powerful simplicial-aware neural networks. In *The twelfth international conference on learning representations*, 2024.

[Hajij *et al.*, 2020] Hajij, Istvan, and Zamzmi. Cell complex neural networks. In *Topological Data Analysis and Beyond Workshop at NeurIPS 2020*, 2020.

[Hajij *et al.*, 2022] Mustafa Hajij, Ghada Zamzmi, Theodore Papamarkou, Nina Miolane, Aldo Guzmán-Sáenz, Karthikeyan Natesan Ramamurthy, Tolga Birdal, Tamal K Dey, Soham Mukherjee, Shreyas N Samaga, et al. Topological deep learning: Going beyond graph data. *arXiv preprint arXiv:2206.00606*, 2022.

[Hajij *et al.*, 2023] Mustafa Hajij, Ghada Zamzmi, Theodore Papamarkou, Aldo Guzman-Saenz, ToIga Birdal, and Michael T Schaub. Combinatorial complexes: Bridging the gap between cell complexes and hypergraphs. In *2023 57th Asilomar Conference on Signals, Systems, and Computers*, pages 799–803. IEEE, 2023.

[He *et al.*, 2025] Xin He, Yili Wang, Wenqi Fan, Xu Shen, Xin Juan, Rui Miao, and Xin Wang. Mamba-based graph convolutional networks: tackling over-smoothing with selective state space. In *Proceedings of the Thirty-Fourth International Joint Conference on Artificial Intelligence, IJCAI ’25*, 2025.

[Huang and Yang, 2021] Jing Huang and Jie Yang. Unignn: a unified framework for graph and hypergraph neural networks. In *Proceedings of the Thirtieth International Joint Conference on Artificial Intelligence*. International Joint Conferences on Artificial Intelligence Organization, 2021.

[Jo *et al.*, 2021] Jaehyeong Jo, Jinheon Baek, Seul Lee, Dongki Kim, Minki Kang, and Sung Ju Hwang. Edge representation learning with hypergraphs. *NeurIPS*, 34:7534–7546, 2021.

[Kipf, 2016] TN Kipf. Semi-supervised classification with graph convolutional networks. *arXiv preprint arXiv:1609.02907*, 2016.

[Lecha *et al.*, 2025] Manuel Lecha, Andrea Cavallo, Francesca Dominici, Elvin Isufi, and Claudio Battiloro. Higher-order topological directionality and directed simplicial neural networks. In *ICASSP 2025-2025 IEEE International Conference on Acoustics, Speech and Signal Processing (ICASSP)*, pages 1–5. IEEE, 2025.

[Lee *et al.*, 2022] See Hian Lee, Feng Ji, and Wee Peng Tay. Sgat: Simplicial graph attention network. In *Proceedings of the Thirty-First International Joint Conference on Artificial Intelligence*. International Joint Conferences on Artificial Intelligence Organization, 2022.

[Love *et al.*, 2023] Ephy R Love, Benjamin Filippenko, Vasileios Maroulas, and Gunnar Carlsson. Topological convolutional layers for deep learning. *Journal of Machine Learning Research*, 24(59):1–35, 2023.

[Morris *et al.*, 2020] Christopher Morris, Nils Morten Kriege, Franka Bause, Kristian Kersting, Petra Mutzel, and Marion Neumann. Tudataset: A collection of benchmark datasets for learning with graphs. In *ICML 2020 Workshop on Graph Representation Learning and Beyond*, 2020.

[Naitzat *et al.*, 2020] Gregory Naitzat, Andrey Zhitnikov, and Lek-Heng Lim. Topology of deep neural networks. *Journal of Machine Learning Research*, 21(184):1–40, 2020.

[Nishikawa and Suzuki, 2025] Naoki Nishikawa and Taiji Suzuki. State space models are provably comparable to transformers in dynamic token selection. In *The Thirteenth International Conference on Learning Representations*, 2025.

[Papamarkou *et al.*, 2024] Theodore Papamarkou, Tolga Birdal, Michael Bronstein, Gunnar Carlsson, Justin Curry, Yue Gao, Mustafa Hajij, Roland Kwitt, Pietro Liò, Paolo Di Lorenzo, et al. Position paper: Challenges and opportunities in topological deep learning. *arXiv preprint arXiv:2402.08871*, 24:25, 2024.

[Papillon *et al.*, 2023] Mathilde Papillon, Sophia Sanborn, Mustafa Hajij, and Nina Miolane. Architectures of topological deep learning: A survey of message-passing topological neural networks. *arXiv preprint arXiv:2304.10031*, 2023.

[Papillon *et al.*, 2025] Mathilde Papillon, Guillermo Bernardez, Claudio Battiloro, and Nina Miolane. Topotune: A framework for generalized combinatorial complex neural networks. In *Forty-second International Conference on Machine Learning*, 2025.

[Pham *et al.*, 2025] Phu Pham, Quang-Thinh Bui, Ngoc Thanh Nguyen, Robert Kozma, Philip S Yu, and Bay Vo. Topological data analysis in graph neural networks: surveys and perspectives. *IEEE Transactions on Neural Networks and Learning Systems*, 2025.

[Platonov *et al.*, 2023] Oleg Platonov, Denis Kuznedelev, Michael Diskin, Artem Babenko, and Liudmila Prokhorenkova. A critical look at the evaluation of gnns under heterophily: Are we really making progress? In *The Eleventh International Conference on Learning Representations*, 2023.

[Roddenberry *et al.*, 2021] T Mitchell Roddenberry, Nicholas Glaze, and Santiago Segarra. Principled simplicial neural networks for trajectory prediction. In *International Conference on Machine Learning*, pages 9020–9029. PMLR, 2021.

[Sieber *et al.*, 2024] Jerome Sieber, Carmen A Alonso, Alexandre Didier, Melanie N Zeilinger, and Antonio Orvieto. Understanding the differences in foundation models: Attention, state space models, and recurrent neural networks. *NeurIPS*, 37:134534–134566, 2024.

[Telyatnikov *et al.*, 2024] Lev Telyatnikov, Guillermo Bernardez, Marco Montagna, Pavlo Vasylenko, Ghada Zamzmi, Mustafa Hajij, Michael T Schaub, Nina Miolane, Simone Scardapane, and Theodore Papamarkou. Topobenchmarkx: A framework for benchmarking topological deep learning. *arXiv preprint arXiv:2406.06642*, 2024.

[Truong and Chin, 2024] Quang Truong and Peter Chin. Weisfeiler and lehman go paths: Learning topological features via path complexes. In *Proceedings of the AAAI Conference on Artificial Intelligence*, volume 38, pages 15382–15391, 2024.

[Vaswani *et al.*, 2017] Ashish Vaswani, Noam Shazeer, Niki Parmar, Jakob Uszkoreit, Llion Jones, Aidan N Gomez, Łukasz Kaiser, and Illia Polosukhin. Attention is all you need. *NeurIPS*, 30, 2017.

[Wang *et al.*, 2024] Chloe Wang, Oleksii Tsepa, Jun Ma, and Bo Wang. Graph-mamba: Towards long-range graph sequence modeling with selective state spaces. *arXiv preprint arXiv:2402.00789*, 2024.

[Wen *et al.*, 2024] Tao Wen, Elynn Chen, and Yuzhou Chen. Tensor-view topological graph neural network. In *International Conference on Artificial Intelligence and Statistics*, pages 4330–4338. PMLR, 2024.

[Wu *et al.*, 2023] Hanrui Wu, Andy Yip, Jinyi Long, Jia Zhang, and Michael K Ng. Simplicial complex neural networks. *IEEE Transactions on Pattern Analysis and Machine Intelligence*, 46(1):561–575, 2023.

[Xu *et al.*, 2018] Keyulu Xu, Weihua Hu, Jure Leskovec, and Stefanie Jegelka. How powerful are graph neural networks? In *International Conference on Learning Representations*, 2018.

[Yadati *et al.*, 2019] Naganand Yadati, Madhav Nimishakavi, Prateek Yadav, Vikram Nitin, Anand Louis, and Partha Talukdar. Hypergen: A new method for training graph convolutional networks on hypergraphs. In *Advances in Neural Information Processing Systems (NeurIPS) 32*, pages 1509–1520. Curran Associates, Inc., 2019.

[Yang *et al.*, 2016] Zhilin Yang, William Cohen, and Ruslan Salakhudinov. Revisiting semi-supervised learning with graph embeddings. In *International conference on machine learning*, pages 40–48. PMLR, 2016.

[Yang *et al.*, 2022] Ruochen Yang, Frederic Sala, and Paul Bogdan. Efficient representation learning for higher-order data with simplicial complexes. In *Learning on Graphs Conference*, pages 13–1. PMLR, 2022.

[Yuan *et al.*, 2025] Haonan Yuan, Qingyun Sun, Zhaonan Wang, Xingcheng Fu, Cheng Ji, Yongjian Wang, Bo Jin, and Jianxin Li. Dg-mamba: Robust and efficient dynamic graph structure learning with selective state space models. In *Proceedings of the AAAI Conference on Artificial Intelligence*, volume 39, pages 22272–22280, 2025.

A Related Work

Higher-order Graph Neural Networks. To capture higher-order interactions beyond pairwise graphs, higher-order models have been developed. Hypergraph neural networks enable node–hyperedge message passing [Feng *et al.*, 2019; Ding *et al.*, 2020; Cai *et al.*, 2022], but are limited to node–hyperedge relations. Simplicial and cellular neural networks leverage boundary and co-boundary operators to model higher-order interactions. [Roddenberry *et al.*, 2021; Lecha *et al.*, 2025; Wu *et al.*, 2023; Bodnar *et al.*, 2021; Bodnar, 2023]. Combinatorial Complexes [Hajij *et al.*, 2022; Hajij *et al.*, 2023] unify these structures into a single hierarchical framework, aiming for graph representation [Papillon *et al.*, 2023; Papillon *et al.*, 2025]. However, most studies often oversimplify the topologies to hypergraphs or simplicial complexes, limiting their ability to the long-range dependencies.

Graph Mamba. Selective state-space models (SSMs), particularly the Mamba architecture, have emerged as a compelling alternative to transformer for sequence modeling [Dao and Gu, 2024; Yuan *et al.*, 2025]. Mamba achieves linear-time inference through input-dependent state transitions while retaining strong long-range modeling capacity. Motivated by these advantages, [Wang *et al.*, 2024] firstly introduces mamba on graph by integrating a Mamba block with the input-dependent node selection mechanism. [Wang *et al.*, 2024; He *et al.*, 2025; Behrouz and Hashemi, 2024] explore Mamba-based architectures for structured data, and adapt SSMs to graph sequences. These models display improved scalability and long-range dependency modeling but relying on graph neural networks. current graph Mamba methods are confined to pairwise graph structures and overlook higher-order interactions, necessitating their extension to higher-order topological domains with more robust message-passing mechanisms.

B Experiments Detail

B.1 Dataset

- **MUTAG:** This dataset comprises a collection of nitroaromatic compounds, where nodes represent atoms labelled by atomic type, and edges denote the corresponding bonds between atoms.
- **PROTEINS:** This dataset comprises proteins classified as either enzymatic or non-enzymatic. Nodes represent amino acids, and if the distance between two nodes is less than 6 \AA ($1 \text{ \AA} = 10^{-10} \text{ m}$), they are connected.
- **IMDB-BINARY & IMDB-MULTI:** These two datasets are film collaboration datasets, comprising self-directed networks of actors/actresses who have roles in films listed on IMDB. Nodes represent actors/actresses, while edges denote their appearances in the same film. In IMDB-BINARY, edges are drawn from action and romantic films, and in IMDB-MULTI, edges are drawn from comedies, romantic films, and science fiction films.
- **AMAZON-RATINGS:** This dataset consists of Amazon product co-purchase network metadata, where nodes represent products and edges denote items frequently purchased together.

- **ROMAN-EMPIRE:** This dataset is based on the English Wikipedia article Roman Empire, where a node represents a word in the text. An edge is established if two words appear consecutively in the text or are connected in the dependency tree of a sentence.
- **MINESWEEPER:** This dataset is inspired by the Minesweeper game, where each node corresponds to a grid square in the game. Each square connects to its eight neighbours, forming a set of edges.
- **Cora, CiteSeer, and PubMed:** These three datasets serve as benchmark datasets for node classification. Each node represents a document, while edges denote citation relationships between documents.

Datasets	Nodes	Edges	Features	Classes
MUTAG	3371	3371	7	2
PROTEINS	43471	81044	3	2
IMDB-BINARY	19770	193100	0	2
IMDB-MULTI	19500	98910	0	3
AMAZON-RATINGS	24492	93050	300	5
ROMAN-EMPIRE	22662	32927	300	18
MINESWEEPER	10000	39402	7	2
Cora	2708	10556	1433	7
CiteSeer	3327	9104	3703	6
PubMed	19717	88648	500	3

Table 5: Dataset statistics

B.2 Baselines

- **GCN** [Kipf, 2016]: Graph Convolutional Networks that enhance stability and scalability via first-order approximations of spectral graph convolutions.
- **GAT** [Vaswani *et al.*, 2017]: Graph Attention Networks that aggregate neighbor features using attention weights reflecting contextual importance.
- **GIN** [Xu *et al.*, 2018]: A maximally expressive GNN rooted in graph isomorphism theory, using learnable aggregators to capture neighborhood structure for node- and graph-level tasks.
- **HyperGCN** [Yadati *et al.*, 2019]: A hypergraph GNN that treats hyperedges as aggregation units and updates node representations through weighted intra-hyperedge feature aggregation to model higher-order interactions.
- **HyperGAT** [Ding *et al.*, 2020]: Extends attention mechanisms to hypergraphs by computing attention scores within hyperedges to capture multi-node dependencies.
- **UniGCN** **UniGNNII** **UniSAGE** and **UniGIN** [Huang and Yang, 2021]: This is a family of unified GNNs for graphs and hypergraphs that share a common neighborhood aggregation framework. They incorporate graph-specific designs (e.g., residual connections in UniGNNII, SAGE-style sampling in UniSAGE, or GIN-style injectivity in UniGIN) to handle heterogeneous structures while mitigating over-smoothing in deep layers.
- **AllSet** [Chien *et al.*, 2021]: A general hypergraph neural network based on multiset functions, integrating Deep Sets and Set Transformers with permutation-invariant aggregators to flexibly model higher-order relations.

- **EDGNN** [Jo *et al.*, 2021]: A message-passing GNN for directed, edge-labeled graphs that jointly encodes node features, edge labels, and directionality during neighborhood aggregation.
- **SCCN and SCCNN** [Yang *et al.*, 2022]: Simplicial complex networks that learn representations over relaxed simplex complexes without dimensional constraints, enabling superior performance on simplex-level tasks.
- **SGAT** [Lee *et al.*, 2022]: A higher-order GNN for heterogeneous graphs that models multi-objective interactions via pure simplicial complexes and aggregates neighborhoods using multi-head attention.
- **SCN** [Roddenberry *et al.*, 2021; Lecha *et al.*, 2025]: A simplicial convolutional network satisfying directional invariance, and simplex awareness.
- **SANN** [Gurugubelli and Chepuri, 2024]: An efficient simplicial network that reduces training cost and memory usage via pre-aggregation and nonlinear transformations while preserving expressivity.
- **CCNN CXN** [Hajij *et al.*, 2020]: Cellular complex networks that generalize GCN-style convolutions to cellular structures. CCNN uses normalized cellular adjacency, while CXN supports hierarchical cross-cell messaging and handles both directed and undirected complexes.
- **CWN** [Bodnar *et al.*, 2021]: A Weisfeiler–Leman-inspired framework on regular CW complexes that enhances expressivity and long-range dependency modeling via cellular message passing and graph elevation.
- **CCCN** [Papillon *et al.*, 2025]: A foundational topological deep learning model that leverages combinatorial complex representations to capture arbitrary higher-order interactions and hierarchical relationships.

B.3 Experiment Setups

Method	Hyper-parameters set
CCMamba-(graph, hypergraph, simplex, cellular)	hidden:128, batch size:128, layer num:2, state dim:16, expand:2, lr:0.1, dropout:0.01, seed:0,3,5,7,9
CCMultiMamba-(graph, hypergraph, simplex, cellular)	hidden:128, heads:4, batch size:128, layer num:2, state dim:16, expand:2, lr:0.1, dropout:0.01, seed:0,3,5,7,9
CCMamba-(GIN)	hidden:128, batch size:128, layer num:2, state dim:16, expand:2, lr:0.1, dropout:0.01, seed:0,3,5,7,9

Table 6: The model hyper-parameters for experiments.

B.4 Supplementary Results

Table 7 supplements the report with test accuracy of CC-Mamba for multi-head mamba at 2, 4, 8, and 16 heads in four topologies (graph, hypergraph, simplex, and rank cell), covering both graph-level and node-level benchmarks.

Datasets	Models	Layers			
		2	4	8	16
CCMamba-graph	MUTAG	89.15±0.56	76.60±4.05	80.85±7.69	74.47±3.58
	PROTEINS	75.99±1.53	77.06±2.65	77.06±1.93	79.21±2.60
	IMDB-B	74.00±4.69	73.20±2.94	74.00±3.26	73.60±2.69
	IMDB-M	50.93±2.16	53.87±3.36	54.93±3.87	50.67±3.12
	ROMAN-E	85.14±0.63	84.17±0.20	84.01±0.23	84.15±0.26
	AMAZON-R	53.98±0.76	53.45±0.87	52.67±0.81	53.70±0.84
	Minesweeper	85.88±0.56	86.60±0.93	85.92±0.67	85.88±0.46
	Cora	85.97±1.16	85.52±1.03	84.93±1.15	85.97±1.15
	Citeseer	74.31±1.26	74.55±0.93	74.79±1.53	75.51±1.84
	PubMed	89.47±0.28	89.55±0.21	89.47±0.07	89.57±0.31
CCMamba-hypergraph	MUTAG	76.60±3.84	76.60±4.85	78.72±9.30	78.72±4.56
	PROTEINS	74.55±2.50	74.55±2.50	75.27±2.06	77.78±1.63
	IMDB-B	73.20±1.84	72.40±2.93	71.20±2.38	75.20±4.18
	IMDB-M	52.53±2.40	52.00±1.63	53.87±2.91	53.33±3.94
	ROMAN-E	82.05±0.32	80.96±0.42	79.69±0.06	78.77±0.26
	AMAZON-R	51.53±0.67	50.94±0.67	51.36±0.62	52.02±1.03
	Minesweeper	80.84±0.86	83.20±1.84	83.96±0.59	83.68±1.92
	Cora	87.44±0.69	87.89±0.83	88.63±1.01	88.77±1.32
	Citeseer	77.31±1.82	76.71±1.20	77.31±1.25	77.19±1.86
	PubMed	89.57±0.40	89.59±0.42	89.88±0.53	89.72±0.48
CCMamba-simplex	MUTAG	85.11±9.74	80.85±11.39	76.60±4.95	72.34±5.06
	PROTEINS	73.12±3.60	72.76±1.49	72.76±1.09	71.68±1.53
	IMDB-B	75.20±3.69	71.20±2.65	68.80±0.57	69.25±0.53
	IMDB-M	44.53±5.70	35.20±0.89	42.67±5.09	48.27±11.50
	ROMAN-E	82.46±0.91	81.26±0.59	80.50±1.32	80.74±1.54
	AMAZON-R	48.57±0.86	47.84±4.30	46.96±2.72	47.27±1.96
	Minesweeper	82.32±1.49	82.76±2.30	82.20±1.37	82.61±1.96
	Cora	67.65±4.93	40.62±3.17	44.31±6.25	54.95±10.37
	Citeseer	65.55±3.70	51.62±9.48	50.66±7.84	45.02±2.63
	PubMed	86.88±0.47	87.63±0.42	85.96±3.30	85.86±17.93
CCMamba-rank-cell	MUTAG	80.85±5.64	76.60±4.58	80.85±4.16	82.98±3.85
	PROTEINS	78.14±2.39	77.42±2.65	77.78±3.15	77.78±2.69
	IMDB-B	72.00±2.15	72.80±2.31	72.80±1.36	72.80±1.08
	IMDB-M	51.20±2.68	53.87±2.96	49.33±1.72	51.47±2.93
	ROMAN-E	85.70±0.69	85.42±0.21	85.51±0.40	84.86±0.27
	AMAZON-R	48.88±1.15	49.98±0.83	49.11±0.65	48.83±0.69
	Minesweeper	83.32±0.67	83.92±0.65	83.96±0.65	83.96±0.57
	Cora	89.51±1.63	88.04±0.83	88.48±0.62	88.18±0.92
	Citeseer	76.71±1.23	77.19±1.58	77.07±1.82	77.43±1.78
	PubMed	88.82±0.49	88.86±0.45	88.97±0.53	89.15±0.56

Table 7: Test accuracy (%) of MultiMamba with different heads number (e.g., 2,4,8,16) on node-level and graph-level tasks.

Table 8 reports graph-level test accuracies of GAT, Mamba, MultiGAT, and MultiMamba across four datasets under four higher-order structures (graph, hypergraph, simplex, cellular). All models share the same backbone and neighborhood construction—only the aggregation mechanism differs. Mamba consistently matches or exceeds GAT, especially on IMDB-B and ROMAN-E with non-graph structures (e.g., +6.2% on IMDB-B hypergraphs). MultiMamba achieves the best overall performance on ROMAN-E (87.12% with cellular structure). In contrast, attention-based methods degrade notably on higher-order representations (e.g., GAT drops to 34.67% on IMDB-B hypergraphs). These results highlight the effectiveness of selective state-space aggregation.

C Proof for Theorem

Proposition 3 ((1-CCWL)). *If 1-CCWL test decides \mathcal{CC}_1 and \mathcal{CC}_2 are non-isomorphic, then $\mathcal{CC}_1 \neq \mathcal{CC}_2$.*

Proof for Proposition 3. We prove the contrapositive. Assume that \mathcal{CC}_1 and \mathcal{CC}_2 are isomorphic combinatorial complexes. Let $\mathcal{CC}_1 = (\mathcal{S}_1, \mathcal{C}_1, \text{rk})$ and $\mathcal{CC}_2 = (\mathcal{S}_2, \mathcal{C}_2, \text{rk})$.

	Dataset	Structure	GAT	Mamba	MultiGAT	MultiMamba
IMDB-B	Graph	68.40±3.73	73.20±3.50	70.40±1.51	72.43±1.19	
	Hypergraph	34.67±2.08	72.40±2.60	68.40±2.82	72.17±4.28	
	Simplex	45.35±2.83	71.20±2.91	71.04±2.71	72.80±3.65	
	Cellular	68.62±3.07	74.81±1.85	70.01±2.05	72.40±1.12	
ROMAN-E	Graph	83.25±1.82	83.46±2.40	79.61±2.45	78.43±1.53	
	Hypergraph	71.56±0.39	78.52±1.80	75.57±2.61	77.25±2.28	
	Simplex	84.70±2.79	85.51±1.24	84.42±5.14	83.91±1.82	
	Cellular	84.30±1.85	85.49±1.72	86.02±1.84	87.12±2.79	
AMAZON-R	Graph	49.29±3.94	52.92±2.85	50.20±0.95	50.86±1.28	
	Hypergraph	48.11±0.16	49.53±2.23	45.21±1.53	48.75±2.84	
	Simplex	48.99±3.41	48.90±3.53	49.50±2.19	49.20±2.80	
	Cellular	49.50±3.20	50.34±2.74	49.36±2.37	49.18±1.86	
Minesweeper	Graph	83.84±1.01	85.52±1.10	84.96±2.10	82.20±3.52	
	Hypergraph	79.82±0.49	83.48±1.05	79.60±3.16	81.05±2.77	
	Simplex	82.84±2.41	81.12±1.82	82.50±0.85	79.52±1.62	
	Cellular	84.20±1.10	84.57±3.10	84.21±4.02	84.88±1.46	

Table 8: Test accuracy (%) of GAT, Mamba, MultiGAT, and MultiMamba on graph-level tasks.

By isomorphism definition, there exists an injection function $\varphi : \mathcal{CC}_1 \rightarrow \mathcal{CC}_2$. For all $\sigma \in \mathcal{CC}_1$, the ranks are preserved: $\text{rk}(\sigma) = \text{rk}(\varphi(\sigma))$ (i.e., nodes map to nodes, edges to edges, faces to faces). Moreover, the incidence matrix is preserved: for each cell $\sigma \in \mathcal{CC}_1$, the sets of incident nodes, edges and faces correspond under φ . It holds $\varphi(E_v) = E_{\varphi(v)}$, $\varphi(V_e) = V_{\varphi(e)}$, $\varphi(F_e) = F_{\varphi(e)}$, $\varphi(E_f) = E_{\varphi(f)}$. We show by induction on k that the labels produced by the 1-CCWL refinement are preserved under φ at every iteration, i.e., for all $\sigma \in \mathcal{CC}_1$, $k \geq 0$, there holds $\ell_{\mathcal{CC}_2, \varphi(\sigma)}^{(k)} = \ell_{\mathcal{CC}_1, \sigma}^{(k)}$.

At $k = 0$, By definition, all nodes, edges and faces are initialized with the same labels $\ell_v^{(0)}, \ell_e^{(0)}, \ell_f^{(0)} = 0$ in both complexes, so that $\ell_{\mathcal{CC}_2, \varphi(\sigma)}^{(0)} = \ell_{\mathcal{CC}_1, \sigma}^{(0)}$.

For some $k \geq 0$, we suppose that labels at iteration k are preserved under φ . Then we conclude that it also holds for iteration $k + 1$ for nodes, edges and faces.

We employ the 1-CCWL update rule on two combinatorial complexes. For the node $v \in \mathcal{CC}_1$, we have $\ell_v^{(k+1)} = \{\{\ell_v^{(k)}\}, \{\{\ell_e^{(k)}\}_{e \in E_v}\}\}$. Since φ is an isomorphism preserving incidence and, by the induction hypothesis, $\ell_{\mathcal{CC}_2, \varphi(x)}^{(k)} = \ell_{\mathcal{CC}_1, x}^{(k)}$ for all cells x , the multiset $\{\{\ell_e^{(k)}\}_{e \in E_v}\}$ in \mathcal{CC}_1 coincides with $\{\{\ell_{e'}^{(k)}\}_{e' \in E_{\varphi(v)}}\}$ in \mathcal{CC}_2 . Hence $\ell_{\mathcal{CC}_2, \varphi(v)}^{(k+1)} = \ell_{\mathcal{CC}_1, v}^{(k+1)}$. The same argument applies to edges and faces. For an edge e , $\ell_e^{(k+1)} = \{\{\ell_e^{(k)}\}, \{\{\ell_v^{(k)}\}_{v \in V_e}\}, \{\{\ell_f^{(k)}\}_{f \in F_e}\}\}$, and the isomorphism φ preserves both V_e and F_e as well as all labels at iteration k , so $\ell_{\mathcal{CC}_2, \varphi(e)}^{(k+1)} = \ell_{\mathcal{CC}_1, e}^{(k+1)}$. For a face f , we also have $\ell_f^{(k+1)} = \{\{\ell_f^{(k)}\}, \{\{\ell_e^{(k)}\}_{e \in E_f}\}\}$, and again the incidence-preserving property of φ and the induction hypothesis imply $\ell_{\mathcal{CC}_2, \varphi(f)}^{(k+1)} = \ell_{\mathcal{CC}_1, f}^{(k+1)}$. Thus, by induction, for every iteration k and every cell $\sigma \in \mathcal{C}_1$, the labels of σ and $\varphi(\sigma)$ coincide. In particular, the multisets of labels in \mathcal{CC}_1 and \mathcal{CC}_2 are identical at each iteration k :

$$\{\{\ell_{\mathcal{CC}_1, \sigma_1}^{(k)} : \sigma_1 \in \mathcal{CC}_1\} = \{\{\ell_{\mathcal{CC}_2, \sigma_2}^{(k)} : \sigma_2 \in \mathcal{CC}_2\}\}.$$

Therefore, the 1-CCWL test cannot distinguish isomorphic combinatorial complexes. Taking the contrapositive, if the

1-CCWL test distinguishes \mathcal{CC}_1 and \mathcal{CC}_2 , there exists a cell at k -iteration such that $\{\{\ell_{\mathcal{CC}_1, \sigma_1}^{(k)} : \sigma_1 \in \mathcal{CC}_1\} \neq \{\{\ell_{\mathcal{CC}_2, \sigma_2}^{(k)} : \sigma_2 \in \mathcal{CC}_2\}\}$, then \mathcal{CC}_1 and \mathcal{CC}_2 are not isomorphic. \square

Therefore, we can conclude that 1-CCWL distinguish \mathcal{CC}_1 and \mathcal{CC}_2 as non-isomorphic if there exists a cell at k -iteration such that the condition

$$\{\{\ell_{\mathcal{CC}_1, \sigma_1}^{(k)} : \sigma_1 \in \mathcal{CC}_1\} \neq \{\{\ell_{\mathcal{CC}_2, \sigma_2}^{(k)} : \sigma_2 \in \mathcal{CC}_2\}\}, \quad (14)$$

Lemma 2. Suppose an injective function $\mathcal{A} : \mathcal{CC}_1 \rightarrow \mathcal{CC}_2$, and let the labels $\ell_{\mathcal{CC}}^{(k)} = \{\ell_v^{(k)}, \ell_e^{(k)}, \ell_f^{(k)}\}$, and features $h_{\mathcal{CC}}^{(k)} = \{h_v^{(k)}, h_e^{(k)}, h_f^{(k)}\}$ of node, edge and face in combinatorial complex \mathcal{CC} at iteration k , respectively. If the conditions hold,

$$\begin{cases} l_{\mathcal{CC}_1, \sigma_1}^{(j)} = l_{\mathcal{CC}_2, \sigma_2}^{(j)}, & \forall j \leq k \\ h_{\mathcal{CC}_1, \sigma_1}^{(j)} = h_{\mathcal{CC}_2, \sigma_2}^{(j)}, & \forall j \leq k-1 \end{cases} \quad (15)$$

for iterations $0, 1, \dots, k$. Then, for the condition in Equation 14 holds, it follows that $h_{\mathcal{CC}_1, \sigma_1}^{(k)} = h_{\mathcal{CC}_2, \sigma_2}^{(k)}$ at iterations k .

Proof of Lemma 2. We prove this condition by induction on the iteration k . At iteration $k = 0$, all cells are initialized with the same feature vector. By assumption, the initial labels coincide, then the statement holds for $k = 0$.

Suppose that the claim holds for iterations $\forall j \leq k - 1$, i.e., for any pair of cells $\sigma_1 \in \mathcal{CC}_1, \sigma_2 \in \mathcal{CC}_2$ with $\ell_{\mathcal{CC}_1, \sigma_1}^{(j)} = \ell_{\mathcal{CC}_2, \sigma_2}^{(j)}$. In the case of the function \mathcal{A} is an injective function, we also have $h_{\mathcal{CC}_1, \sigma_1}^{(j)} = h_{\mathcal{CC}_2, \sigma_2}^{(j)}$, where the cells σ_1, σ_2 can be nodes (0-cells), edges (1-cells), and faces (2-cells).

Let E_v be the set of incident edges of a node v , V_e, F_e the incident nodes and faces of an edge e , and E_f the incident edges of a face f . For an iteration k and a pair of cells $\sigma_1 \in \mathcal{CC}_1, \sigma_2 \in \mathcal{CC}_2$ such that $\ell_{\mathcal{CC}_1, \sigma_1}^{(k)} = \ell_{\mathcal{CC}_2, \sigma_2}^{(k)}$. By the definition of the 1-CCWL update rule, this implies that:

$$\begin{aligned} & \{\{\ell_v^{(k-1)}\}_{v \in E_v(\sigma_1)}, \{\{\ell_e^{(k-1)}\}_{e \in V_e(\sigma_1) \cup F_e(\sigma_1)}, \{\{\ell_f^{(k-1)}\}_{f \in E_f(\sigma_1)}\} \\ &= \{\{\ell_v^{(k-1)}\}_{v \in E_v(\sigma_2)}, \{\{\ell_e^{(k-1)}\}_{e \in V_e(\sigma_2) \cup F_e(\sigma_2)}, \{\{\ell_f^{(k-1)}\}_{f \in E_f(\sigma_2)}\}. \end{aligned} \quad (16)$$

It indicates that at iteration $k - 1$ the multisets of neighbor labels around σ_1 and σ_2 coincide. By the inductive hypothesis, equality of labels up to iteration $k - 1$ implies equality of features up to iteration $k - 1$. Consequently, the above multiset equalities also hold at the feature level.

$$\begin{aligned} & \{\{h_v^{(k-1)}\}_{v \in E_v(\sigma_1)}, \{\{h_e^{(k-1)}\}_{e \in V_e(\sigma_1) \cup F_e(\sigma_1)}, \{\{h_f^{(k-1)}\}_{f \in E_f(\sigma_1)}\} \\ &= \{\{h_v^{(k-1)}\}_{v \in E_v(\sigma_2)}, \{\{h_e^{(k-1)}\}_{e \in V_e(\sigma_2) \cup F_e(\sigma_2)}, \{\{h_f^{(k-1)}\}_{f \in E_f(\sigma_2)}\}. \end{aligned} \quad (17)$$

By construction, the CCMamba layer \mathcal{A} updates $h_{\sigma}^{(k)}$ through injective projection and permutation-invariant aggregation over these neighbor-feature multisets (at cell level) together with the previous feature of σ itself. Since all these

inputs coincide for σ_1 and σ_2 at iteration $k - 1$, the injectivity of \mathcal{A} implies $h_{CC_1, \sigma_1}^{(k)} = h_{CC_2, \sigma_2}^{(k)}$. This completes the induction and proves the lemma. \square

Proposition 4. *Given two non-isomorphic combinatorial complexes CC_1 and CC_2 , if \mathcal{A} can distinguish them by $\mathcal{A}(CC_1) \neq \mathcal{A}(CC_2)$, then 1-CCWL test also decides $CC_1 \neq CC_2$.*

Proof of Proposition 4. For the condition that combinatorial complexes CC_1 and CC_2 are non-isomorphic, and \mathcal{A} can distinguish them by $\mathcal{A}(CC_1) \neq \mathcal{A}(CC_2)$.

Let the labels $\ell_{CC}^{(k)} = \{\ell_v^{(k)}, \ell_e^{(k)}, \ell_f^{(k)}\}$, and features $h_{CC}^{(k)} = \{h_v^{(k)}, h_e^{(k)}, h_f^{(k)}\}$ of node, edge and face in combinatorial complex CC at iteration k , respectively. We obtain that there exists k satisfies that:

$$\begin{cases} l_{CC_1, \sigma_1}^{(j)} = l_{CC_2, \sigma_2}^{(j)}, & \forall j \leq k-1 \\ h_{CC_1, \sigma_1}^{(j)} = h_{CC_2, \sigma_2}^{(j)}, & \forall j \leq k-1 \\ h_{CC_1, \sigma_1}^{(k)} \neq h_{CC_2, \sigma_2}^{(k)} \end{cases} \quad (18)$$

If we suppose that 1-CCWL test cannot distinguish CC_1, CC_2 , It indicates that at iteration k holds

$$\begin{aligned} & \{\{\ell_v^{(k)}\}\}_{v \in E_v(\sigma_1)}, \{\{\ell_e^{(k)}\}\}_{e \in V_e(\sigma_1) \cup F_e(\sigma_1)}, \{\{\ell_f^{(k)}\}\}_{f \in E_f(\sigma_1)} \\ = & \{\{\ell_v^{(k)}\}\}_{v \in E_v(\sigma_2)}, \{\{\ell_e^{(k)}\}\}_{e \in V_e(\sigma_2) \cup F_e(\sigma_2)}, \{\{\ell_f^{(k)}\}\}_{f \in E_f(\sigma_2)} \end{aligned} \quad (19)$$

which concludes that $l_{CC_1, \sigma_1}^{(k)} = l_{CC_2, \sigma_2}^{(k)}$. According to the Lemma 2, $h_{CC_1, \sigma_1}^{(k)} = h_{CC_2, \sigma_2}^{(k)}$. This contradicts the assumption of formula 19. Thus, the proof of the Proposition finished. \square

Theorem 2. *Given two non-isomorphic combinatorial complexes CC_1 and CC_2 , a CCMamba Layer \mathcal{A} can distinguish them, if conditions hold. Under the conditions of Lemma 2 and with an injective permutation-invariant readout*

1. Local Level. ϕ_1, ϕ_2 functions are injective.
2. Global Level. In addition to the local-level conditions, \mathcal{A} 's graph-level READOUT function is injective.

Proof of Theorem 2. By Proposition 4, the distinguishing power of any CCMamba layer \mathcal{A} is upper-bounded by 1-CCWL test. If a CCMamba layer \mathcal{A} distinguishes CC_1 and CC_2 , then 1-CCWL distinguishes them as well. It remains to prove the converse: if 1-CCWL distinguishes two complexes, then there exists a CCMamba layer (satisfying the stated injectivity assumptions) that distinguishes them.

We first demonstrate that the CCMamba layer can fit the mapping of the 1-CCWL test. Assume 1-CCWL distinguishes CC_1 and CC_2 , there exists an iteration k such that the multisets of 1-CCWL labels are not equal:

$$\{\{\ell_{CC_1, \sigma}^{(k)} : \sigma_1 \in CC_1\}\} \neq \{\{\ell_{CC_2, \sigma}^{(k)} : \sigma_2 \in CC_2\}\}. \quad (20)$$

By induction on $k \in \{0, \dots, K\}$, that one can parameterize the CCMamba layers $\mathcal{A}^{(0)}, \dots, \mathcal{A}^{(k-1)}$ such that at each depth

k there exists an injective map $\Phi^{(k)}$ (i.e., summation function) with for $\forall \sigma \in CC$, we have

$$h_{CC, \sigma}^{(k)} = \Phi^{(k)}(\ell_{CC, \sigma}^{(k)}), \quad (21)$$

which means the feature $h_{\sigma}^{(k)}$ is an injective encoding of the 1-CCWL label $\ell_{\sigma}^{(k)}$. At initialization $k = 0$, all cells of a fixed rank initializes the same label $\ell_{\sigma}^{(0)}$, and the layers initializes all corresponding features $h_{\sigma}^{(0)}$ identically. We can conclude the condition (21) holds for $k = 0$ by defining $\Phi^{(0)}$ to map the (unique) initial label to the initial features.

Assume (21) holds for some $k \geq 0$ with an injective $\Phi^{(k)}$, We prove that there exists a parameterization of $\mathcal{A}^{(k)}$ and an injective $\Phi^{(k+1)}$ such that the condition (21) also holds at iteration $k + 1$. From the perspective of rank definition, we consider cells of different ranks, including nodes, edges, and faces. Within the 1-CCWL, the refined label $\ell_{\sigma}^{(k+1)}$ is obtained by applying an injective map function to the previous label of nodes v , edges e , faces f , and the multisets of labels of incident neighbors, grouped by rank, as follows

$$\begin{aligned} \ell_v^{(k+1)} &= \text{HASH}\left(\ell_v^{(k)}, \{\{\ell_e^{(k)}\}\}_{e \in E_v}\right), \\ \ell_e^{(k+1)} &= \text{HASH}\left(\ell_e^{(k)}, \{\{\ell_v^{(k)}\}\}_{v \in V_e}, \{\{\ell_f^{(k)}\}\}_{f \in E_e}\right), \\ \ell_f^{(k+1)} &= \text{HASH}\left(\ell_f^{(k)}, \{\{\ell_e^{(k)}\}\}_{e \in E_f}\right). \end{aligned} \quad (22)$$

We define the rank neighbor multiset operator $\mathcal{N}_{\tau \rightarrow \sigma, r}^{(k)}(\sigma)$ to be the tuple consisting of the multisets $\{\{\ell_{\tau}^{(k)}\}\}_{\tau \in \mathcal{N}_r(\sigma)}$ for each relevant rank r . Then there exists an injective function η (HASH map), it satisfies

$$\ell_{\sigma}^{(k+1)} = \eta(\ell_{\sigma}^{(k)}, \mathcal{N}_{\tau \rightarrow \sigma, r}^{(k)}(\sigma)). \quad (23)$$

By the inductive hypothesis, $\Phi^{(k)}$ is injective, hence it induces a bijection between labels appearing at depth k and their encoded features. For every σ , the pair $(\ell_{\sigma}^{(k)}, \mathcal{N}_{\tau \rightarrow \sigma, r}^{(k)}(\sigma))$ correspond to the pair $(h_{\sigma}^{(k)}, \hat{\mathcal{N}}_{\tau \rightarrow \sigma}^{(k)}(\sigma))$, where $\hat{\mathcal{N}}_{\tau \rightarrow \sigma}^{(k)}(\sigma)$ is obtained by replacing each neighbor label multiset by the multiset of the corresponding neighbor features.

From local-level assumptions, the CCMamba update $\mathcal{A}^{(k)}$ (i) ϕ_1 maps injectively the per-rank aggregations, and (ii) ϕ_2 combines the fused neighbor summation function with the center feature. Therefore, there exists a update map $(h_{\sigma}^{(k)}, \hat{\mathcal{N}}_{\tau \rightarrow \sigma}^{(k)}(\sigma)) \mapsto h_{\sigma}^{(k+1)}$ is injective as a function of the information in $(\ell_{\sigma}^{(k)}, \mathcal{N}_{\tau \rightarrow \sigma}^{(k)}(\sigma))$. Combining this with (23), we can define an injective map $\Phi^{(k+1)}$ on labels by setting

$$\Phi^{(k+1)}(\ell_{\sigma}^{(k+1)}) := h_{\sigma}^{(k+1)}, \quad (24)$$

which is injective because $h_{\sigma}^{(k+1)}$ is an injective function of $\ell_{\sigma}^{(k+1)}$. Thus the condition (21) holds at depth $k + 1$. By induction, (21) holds for all $k = 0, \dots, K$.

Furthermore, we prove the distinguishability of the CCMamba Layer. Considering the specific CCMamba layer constructed with $h_{CC, \sigma}^{(k)} = \Phi^{(k)}(\ell_{CC, \sigma}^{(k)})$ up to depth K). Suppose

that this layer $\Phi^{(k)}$ cannot distinguish \mathcal{CC}_1 and \mathcal{CC}_2 . Then for $\sigma_1 \in \mathcal{CC}_1, \sigma_2 \in \mathcal{CC}_2$, the final READOUT outputs:

$$\text{READOUT}(\{\{h_{\mathcal{CC}_1, \sigma_1}^{(T)}\}\}) = \text{READOUT}(\{\{h_{\mathcal{CC}_2, \sigma_2}^{(T)}\}\}). \quad (25)$$

By the global-level assumption, READOUT is injective over multisets of cell features, the condition (25) implies the input multisets of features are equal as

$$\{\{h_{\mathcal{CC}_1, \sigma}^{(T)} : \sigma_1 \in \mathcal{CC}_1\}\} = \{\{h_{\mathcal{CC}_2, \sigma}^{(T)} : \sigma_2 \in \mathcal{CC}_2\}\}. \quad (26)$$

Since $\Phi^{(T)}$ is injective and $h_\sigma^{(T)} = \Phi^{(T)}(\ell_\sigma^{(T)})$, equality of feature multisets in (26) implies equality of label multisets:

$$\{\{\ell_{\mathcal{CC}_1, \sigma}^{(T)} : \sigma \in \mathcal{CC}_1\}\} = \{\{\ell_{\mathcal{CC}_2, \sigma}^{(T)} : \sigma \in \mathcal{CC}_2\}\},$$

contradicting (20). Therefore, the constructed CCMamba layer must distinguish \mathcal{CC}_1 and \mathcal{CC}_2 .

Overall, we have proved CCMamba cannot distinguish more pairs than 1-CCWL (Proposition 4), and whenever 1-CCWL distinguishes two complexes, there exists a CCMamba layer (under the stated injectivity assumptions) that distinguishes them. Hence, under the stated conditions, CCMamba and 1-CCWL have exactly the same distinguishing power. \square